

NAVIER-STOKES ANALYSIS OF BLADE TIP SHAPE IN HOVER

Takashi Aoyama
Research Center for Advanced Science and Technology,
University of Tokyo
4-6-1, Komaba, Meguro-ku, Tokyo, Japan 153

Shigeru Saito
National Aerospace Laboratory
7-44-1, Jindaijihigashi-machi, Chofu, Tokyo, Japan 182

Keiji Kawachi
Research Center for Advanced Science and Technology,
University of Tokyo
4-6-1, Komaba, Meguro-ku, Tokyo, Japan 153

Abstract

The three-dimensional Navier-Stokes equations are solved to analyze the flowfield around blade tips of hovering rotors. The eddy viscosity is calculated by employing the $q - \omega$ two-equation turbulence model developed by Coakley. An implicit finite-difference method is used to solve the equations and the algebraic method is adopted to generate the grids. The effect of wake outside of the grid is taken into calculation by correcting the equivalent geometric angle of attack along the blade radius. Its value is estimated by using Local Circulation Method (LCM). The pressure distributions of rectangular tip shape predicted by the present method are in good agreement with the experimental data. The computed results for swept or tapered tip shapes by the present NS code are compared with our Euler results at subsonic condition. Differences between the results obtained by the viscous and inviscid analyses are shown. In addition, the effects of the swept or tapered tip shapes on the performance of helicopter rotor are also analyzed for various tip speed by using our Euler code. Some properties of such the tip shapes are comprehended both in subsonic and transonic conditions.

Introduction

The tip shape of a helicopter blade attracts more and more interest in order to improve the performance of helicopter at high speed range. Westland Lynx made the world speed record (400km/h) of helicopter by using the advanced tip shape called BERP blade[1]. For such a blade tip of high speed helicopter, the transonic shock is generated at the advancing side and the separation occurs at the retreating side of the rotor. In order to analyze the flowfield around high speed helicopter blade tip, following methods have been developed.

The governing equation used in the first stage of the research was the small disturbance potential equation[2] because of its simplicity of the calculation. The governing equations, then, progressed from the full potential equation[3-7] to the Euler equations[8-16]. The advantage of solving the Euler equations instead of the full potential equation is that the Euler equations allow vorticity as well as entropy gradients. By using the Euler equations, however, it is impossible to analyze the viscous-generated phenomena such as shock boundary-layer interaction and separation. The

Navier-Stokes (NS) equations[17-19] are solved to improve the Euler analysis at Georgia Institute of Technology, McDonnell Douglas and NASA Ames Research Center. These analysis use zero-equation algebraic turbulence model. This type of turbulence model can not fully represent the phenomenon of deep separation which occurs at the retreating side of helicopter rotor.

In this study, Euler and NS codes, which were originally developed for the calculation of ATP[20,21], are extended for the analysis of helicopter rotor blades. This Navier-Stokes code has the $q-\omega$ two-equation turbulence model developed by Coakley[22] which can represent the feature of turbulence more precise than zero-equation turbulence model. The flowfield of steady hovering rotor is analyzed as the initial stage of the research by using time marching technique. The induced velocity generated by the vortices outside of the grid is taken into calculation by correcting the equivalent geometric angle of attack along the blade radius. This induced velocity is calculated by using Local Circulation Method (LCM)[23] which has been well applied to predict the aerodynamic performance of helicopter rotor.

The calculated results for a rectangular tip shape of model helicopter rotor are compared with experimental data. In addition, the computed results for swept or tapered tip shapes by the present NS code are compared with the results by our Euler code at a subsonic condition. The effects of the swept or tapered tip shapes on the performance of helicopter rotor analyzed by using the Euler code in transonic conditions are also presented.

Governing Equations

Navier-Stokes Equations

The governing equations are the three-dimensional Reynolds-averaged Navier-Stokes equations in the rotating Cartesian coordinate system (x,y,z) shown in Fig.1. In order to conduct the calculation with arbitrary curved grid, these equations are transformed from the Cartesian coordinate system to the arbitrary curvilinear coordinate system (ξ,η,ζ) shown in Fig.1. The transformed equations are written as

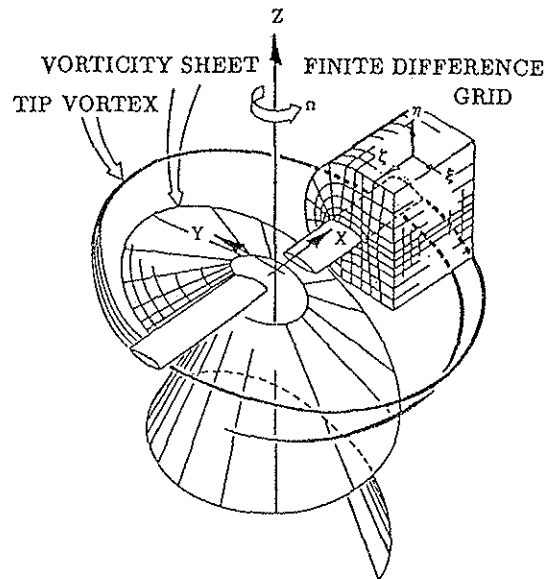


Fig.1 Coordinate system and grid.

$$\frac{\partial Q}{\partial t} + \frac{\partial F_i}{\partial \xi_i} + H = Re^{-1} \frac{\partial S_i}{\partial \xi_i}$$

where

$$Q = J^{-1} \begin{bmatrix} \rho \\ \rho u_1 \\ \rho u_2 \\ \rho u_3 \\ e \end{bmatrix},$$

$$F_i = J^{-1} \begin{bmatrix} \rho U_i \\ \rho u_1 U_i + \xi_{i,1} p \\ \rho u_2 U_i + \xi_{i,2} p \\ \rho u_3 U_i + \xi_{i,3} p \\ (e + p) U_i - \xi_{i,t} p \end{bmatrix},$$

$$H = J^{-1} \begin{bmatrix} 0 \\ -\rho \Omega u_2 \\ \rho \Omega u_1 \\ 0 \\ 0 \end{bmatrix},$$

$$S_i = J^{-1} \begin{bmatrix} 0 \\ \xi_{i,j} \tau_{1j} \\ \xi_{i,j} \tau_{2j} \\ \xi_{i,j} \tau_{3j} \\ \tau_{kj} u_k + q_i \end{bmatrix}$$

In these equations, $()_{,t} = \frac{\partial}{\partial t}$, $()_{,j} = \frac{\partial}{\partial x_j}$, and $(x_1, x_2, x_3) = (x, y, z)$, $(\xi_1, \xi_2, \xi_3) = (\xi, \eta, \zeta)$, $(u_1, u_2, u_3) = (u, v, w)$, $(U_1, U_2, U_3) = (U, V, W)$. The quantity ρ is the density, the quantities u, v and w are the velocity components of Cartesian coordinate system, and the

quantities U, V and W are components of the contravariant velocity. The quantity Ω is the angular velocity of the rotation. The metric terms are conventionally defined as follows.

$$\xi_{i,t} = \Omega_{x_2} \xi_{i,1} - \Omega_{x_1} \xi_{i,2}$$

The quantity p is the pressure which is represented as

$$p = (\gamma - 1) \left[e - \frac{1}{2} \rho u_i^2 \right]$$

where γ is the ratio of specific heats and e is the total energy per unit volume. The variables τ_{ij} and q_i are the stress tensor and the heat flux vector respectively. The hypothesis of eddy-viscosity gives

$$\tau_{ij} = (\mu + \mu_t) (u_{i,j} + u_{j,i} - \frac{2}{3} \delta_{ij} u_{k,k})$$

$$q_i = \left(\frac{\mu}{Pr} + \frac{\mu_t}{Pr_t} \right) \frac{a_{,i}^2}{\gamma - 1}$$

where μ and μ_t are the molecular and turbulent eddy viscosities, and Pr and Pr_t are the laminar and turbulent Prandtl numbers which are assumed to be constant values 0.72 and 0.9 respectively. The quantity J is the Jacobian of the transformation and Re is the Reynolds number based on the rotor radius. The quantity a is the speed of sound.

Turbulence Model

The turbulence eddy viscosity mentioned above is calculated by employing the $q - \omega$ two-equation model developed by Coakley in this section. Both zero-equation model and two-equation model are classified as the eddy viscosity model which defines the Reynolds stresses as a multiple of the eddy viscosity and the mean strain rates in accordance with the Boussinesq's hypothesis.

Although zero-equation models have high numerical compatibility and are effective in attached or weakly separated flows, it is difficult to estimate the algebraic length-scale for complex separated flows. In addition, they are not able to account for flow-history or stress-relaxation effects because of their assumption of equilibrium turbulence.

In contrast, two-equation models over-

come these difficulties because the partial differential equations for both velocity and length scales of the flow are solved. In spite of the assumption of isotropic turbulence, it is verified that two-equation models work well even for anisotropic complex flows including separation.

Though some kinds of two-equation models have been proposed, $q - \omega$ model developed by Coakley is selected here due to its numerical compatibility and practical ability to predict transitional phenomena. The following equations are solved in the $q - \omega$ model in order to get the field variables q and ω which are respectively related to turbulent kinetic energy k and dissipation rate ϵ via $q = \sqrt{k}$ and $\omega = \epsilon/k$.

$$\frac{\partial Q_t}{\partial t} + \frac{\partial F_{ti}}{\partial \xi_i} = Re^{-1} \frac{\partial S_{ti}}{\partial \xi_i} + H_t$$

where

$$Q_t = J^{-1} \begin{bmatrix} \rho q \\ \rho \omega \end{bmatrix}, \quad F_{ti} = J^{-1} \begin{bmatrix} \rho q U_i \\ \rho \omega U_i \end{bmatrix},$$

$$S_{ti} = J^{-1} \begin{bmatrix} (\mu + \frac{\mu_t}{\sigma_q}) g_{ij} \frac{\partial q}{\partial \xi_i} \\ (\mu + \frac{\mu_t}{\sigma_\omega}) g_{ij} \frac{\partial \omega}{\partial \xi_i} \end{bmatrix},$$

$$H_t = J^{-1} \begin{bmatrix} \frac{1}{2} (C_\mu f_\mu \frac{S}{\omega^2} - \frac{2D}{3\omega} - 1) \rho \omega q \\ [C_1 (C_\mu \frac{S}{\omega^2} - \frac{2D}{3\omega}) - C_2] \rho \omega^2 \end{bmatrix}$$

and

$$\mu_t = C_\mu f_\mu Re \frac{\rho q^2}{\omega},$$

$$f_\mu = 1 - \exp(-\alpha R),$$

$$R = \frac{\mu q s}{\rho} Re$$

where s means normal distance from the wall and $g_{ij} = \nabla \xi_i \cdot \nabla \xi_j$. The velocity field D and the strain rate invariant S are represented as

$$D = u_{k,k},$$

$$S = (u_{i,j} + u_{j,i}) u_{i,j} - \frac{2}{3} D^2$$

Turbulence constants used here are

$$C_1 = 0.405 f_\mu + 0.045,$$

$$C_2 = 0.92, \quad C_\mu = 0.09,$$

$$\alpha = 0.0065, \quad \sigma_q = 1.0, \quad \sigma_\omega = 1.3$$

Numerical Method

The numerical method to solve the governing equations is an implicit finite-difference scheme. The Navier-Stokes equations are discretized in the conventional delta form using Euler backward time differencing. A diagonalized ADI method which utilizes an upwind flux-split technique is used for the implicit left-hand-side regarding the spatial differencing. In addition, a higher-order upwind scheme based on TVD by Chakravarthy and Osher[24] is applied for the inviscid terms of the explicit right-hand-side, and the standard second-order central difference is used for the viscous terms of the explicit part. Each ADI operator is decomposed into the product of lower and upper bidiagonal matrices by using diagonally dominant factorization. The TVD scheme has a good capability of capturing the shock without adding artificial dissipations. The transport equations of $q - \omega$ turbulence model are solved by the same method which is used in solving the Navier-Stokes equations because the transport equations are similar to the Navier-Stokes equations.

Grid Generation

For simplicity of the calculation, algebraic method is adopted to generate the grids. These grids consist of $105 \times 51 \times 39$ points for NS calculations and $105 \times 41 \times 27$ points for Euler calculations. On the blade surface, 75×29 and 75×19 points are distributed respectively and the grid is orthogonalized. The minimum grid spacing of η direction is set to 10^{-6} and 10^{-3} respectively.

Boundary Conditions

The grid has six types of boundaries. For simplicity, all boundary conditions are explicitly specified.

On the blade surface, non-slip and adiabatic conditions are applied. All the quantities are set to the values of free stream at the far-field boundaries and they are extrapolated from the interior at the outflow boundary and the inboard station of the blade. The grid has cuts that lie from the trailing edge to the outflow boundary and beyond the blade tip. Along these cuts, the flow properties are

averaged between above and below.

Wake-Correction

It is important to estimate the effect of wake especially for helicopter because the vortices shed from the preceding blade become close to the blade under consideration and because they have strong influence on the blade airloading. However, the computational region used here covers only one blade. The effect of wake outside of the computational region is taken into calculation by correcting the equivalent geometric angle of attack along the blade radius. Its value is estimated by using LCM. In the calculation of LCM, the effect of compressibility is included by using the two-dimensional experimental data of airfoil aerodynamic characteristics obtained in the range from subsonic to transonic[25]. The calculation is conducted in the thrust coefficient input mode in which the collective pitch angle is modified in order to give the same thrust coefficient as the measurement[26].

Results and Discussions

The method described above is applied to analyze the flowfield of a model helicopter rotor in hover. The rotor has two untwisted blades. The aspect ratio is equal to six and the airfoil section is NACA 0012.

Rectangular tip shape

Calculations are performed for the following three cases to a rectangular tip shape.

- (a) subsonic nonlifting case
($\theta_c = 0^\circ$, $M_T = 0.52$, $Re_R = 1.38 \times 10^7$)
- (b) subsonic lifting case
($\theta_c = 8^\circ$, $M_T = 0.44$, $Re_R = 1.17 \times 10^7$)
- (c) transonic lifting case
($\theta_c = 8^\circ$, $M_T = 0.877$, $Re_R = 2.33 \times 10^7$)

The quantity θ_c is collective pitch angle, the quantity M_T is tip Mach number and Re_R is Reynolds number based on the blade radius and tip velocity.

Fig.2(a)-(c) shows the pressure distribution on blade surface for case (a)-(c) respectively. The quantity y/c is the chordwise distance nondimensionalized by chord length and x/R is the radial station nondimensionalized by the blade radius. In these figures, our

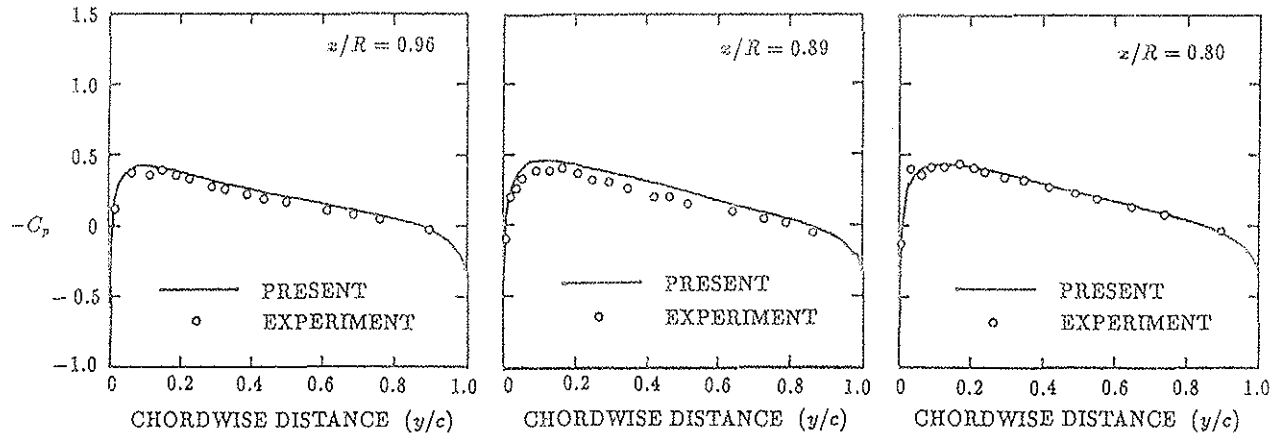


Fig.2(a) Pressure distribution on blade surface for case(a).

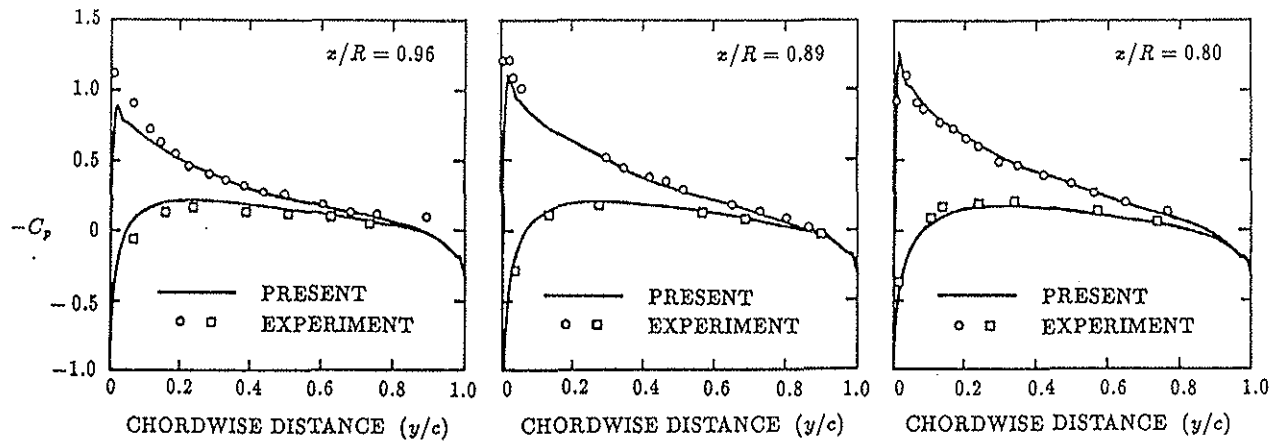


Fig.2(b) Pressure distribution on blade surface for case(b).

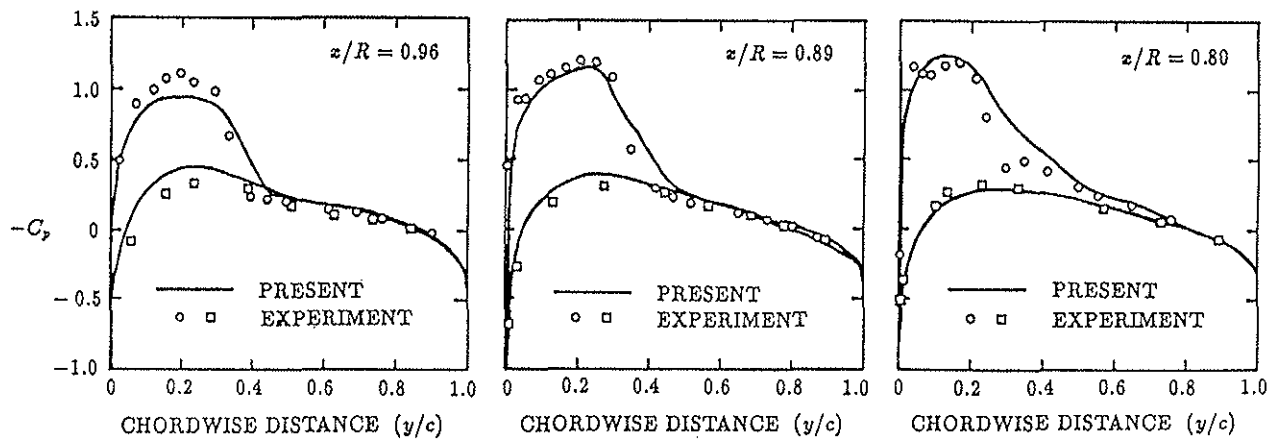


Fig.2(c) Pressure distribution on blade surface for case(c).

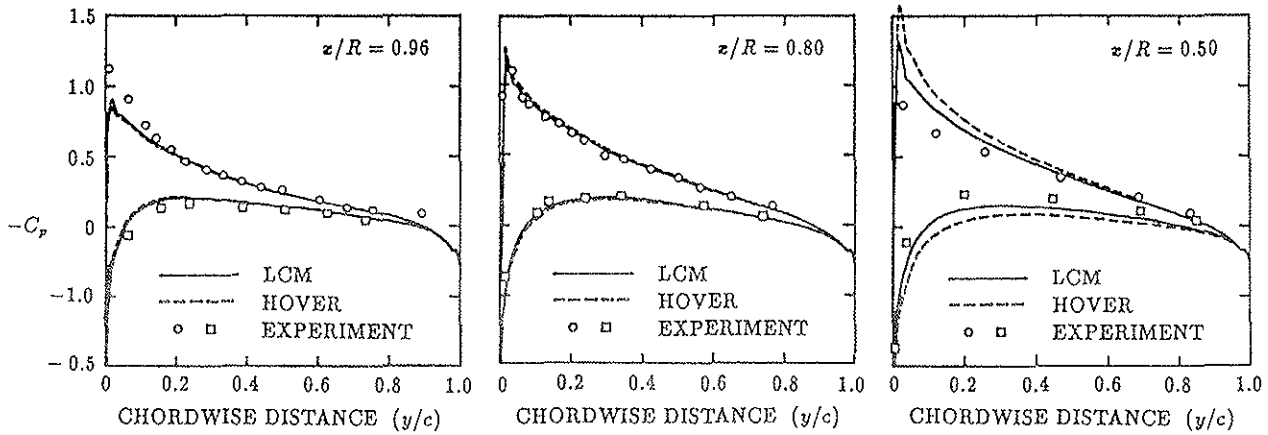


Fig.3 Effect of wake-correction on blade pressure distribution for case(b).

NS results are compared with the experimental data[26]. For lifting case, a constant induced angle of attack 3.8 degree along the entire blade radius is assumed. This induced angle of attack was used in the previous research[17], and is useful for the verification of the present results. Fig.2(a) indicates that the present result for nonlifting case is in good agreement with the experimental data in every radial station. In Fig.2(b), the good agreement with the experimental data is again indicated. However, there is some discrepancy between measured and predicted value near the leading edge. As will be mentioned in the following paragraph, wake-correction has possibility to improve this discrepancy. In Fig.2(c), the present result shows the reasonable prediction even in the transonic condition. These results show that the present computer code has capability to predict the flowfield around blade tip.

The present calculations were performed on FACOM VP-400 vectorized supercomputer at the National Aerospace Laboratory(NAL). It takes about 3 hours to obtain a converged solution which needs about 1500 time steps.

Effect of Wake-correction

Fig.3 shows the difference of the blade surface pressure distribution obtained with the different estimation of wake effects. Calculations are performed for case (b) by using present NS code with the two wake-correction methods. The one uses the constant induced angle of attack 3.8 degree along the entire blade radius. The other is LCM and it gives

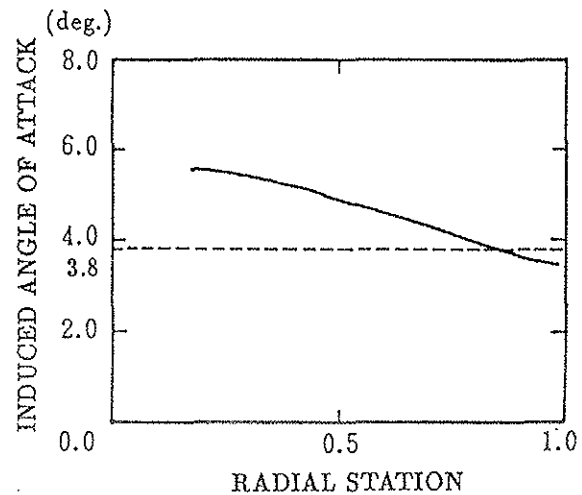


Fig.4 Induced angle of attack along blade radius calculated by using LCM.

the variable induced angle of attack along the blade radius shown in Fig.4. LCM predicts the similar induced angle of attack to 3.8 degree near the blade tip, and larger induced angle of attack near the root. As shown in Fig.3, this difference of the induced angle of attack distribution causes some improvement of the pressure distribution at the mid-radius region. This indicates that the estimation of the wake effect plays important role in this type of calculation.

Regarding to the computational time, it takes only about 20 seconds on the FACOM M-780 scalarcomputer at NAL to obtain the distribution of induced angle of attack by LCM, which is less than 1/10 computational time by our vortex lattice code. It is indicated that LCM is an effective method to estimate the wake effects.

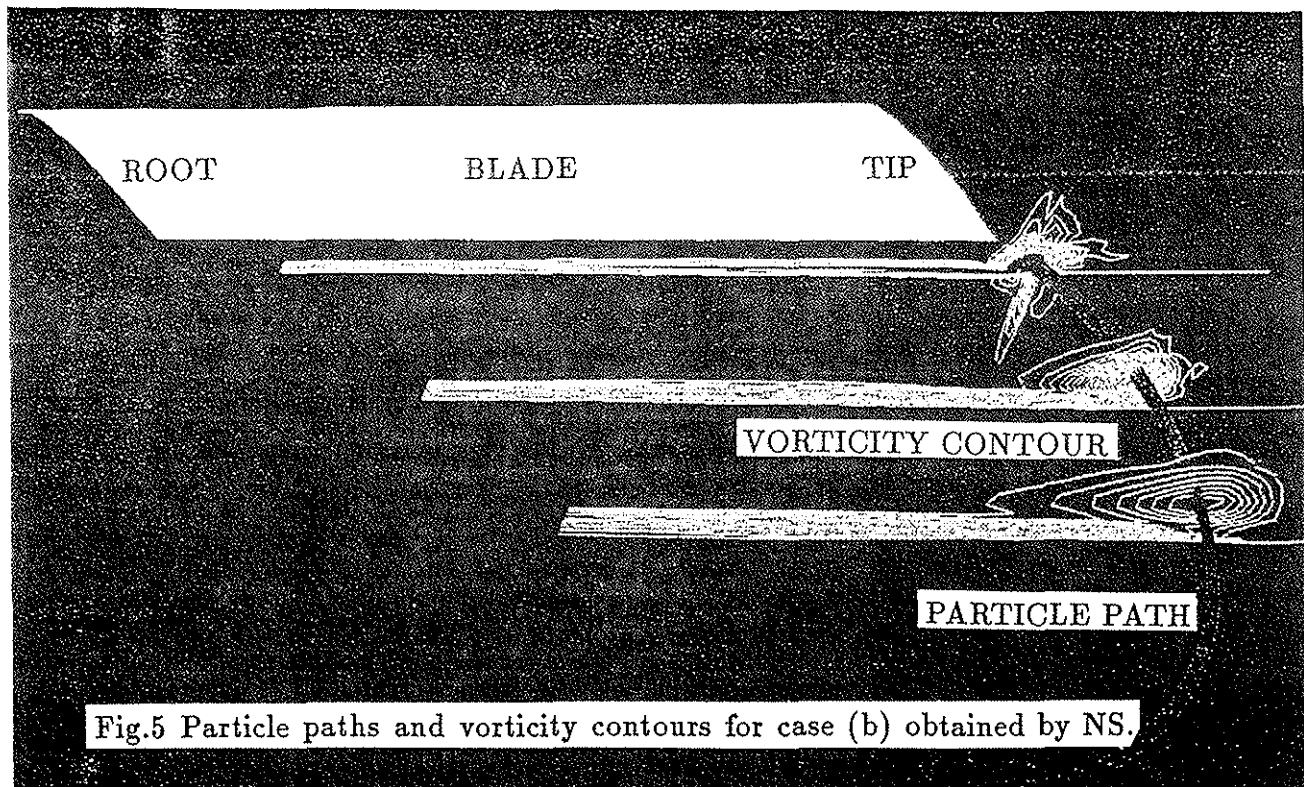


Fig.5 Particle paths and vorticity contours for case (b) obtained by NS.

Wake visualization

Fig.5 shows the tip vortex described by particle paths and vorticity contours behind a blade for case (b) using the wake-correction by LCM. Vorticity contours are obtained in the planes of Fig.6. In this case, the tip vortex is not so clear because of its small effective angle of attack ($\theta_e = 4 - 5 \text{ degree}$). Fig.7 shows the condition of large effective angle of attack ($\theta_e = 14 \text{ degree}$). In this case, the tip vortex can be clearly seen and the difference of descending speed between the tip vortex and inner vorticity sheet is observed. In comparison with the Euler result (Fig.8), the NS result (Fig.7(a)) indicates the more dissipated tip vortex because of viscosity. In addition, the NS results predicts the stronger inner vorticity sheet because it is generated as a result of the viscosity of the boundary-layer. Although the results have not been compared with measurements yet, it is indicated that the feature of the helicopter rotor wake is captured somewhat by the present method. It is, also, observed that the coarse grid in the wake region and conventional boundary conditions should be improved in future.

Modified tip shape

NS analysis So far, our interests are

3rd PLANE

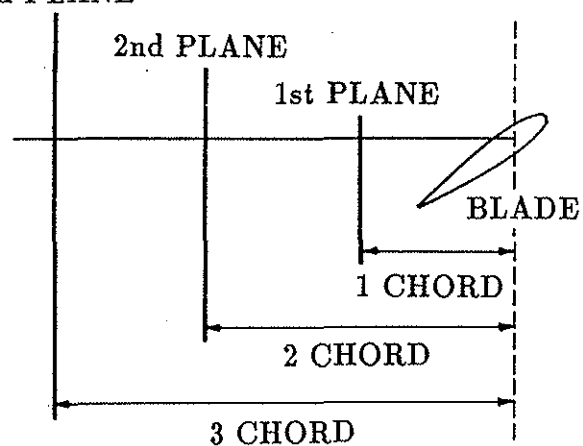
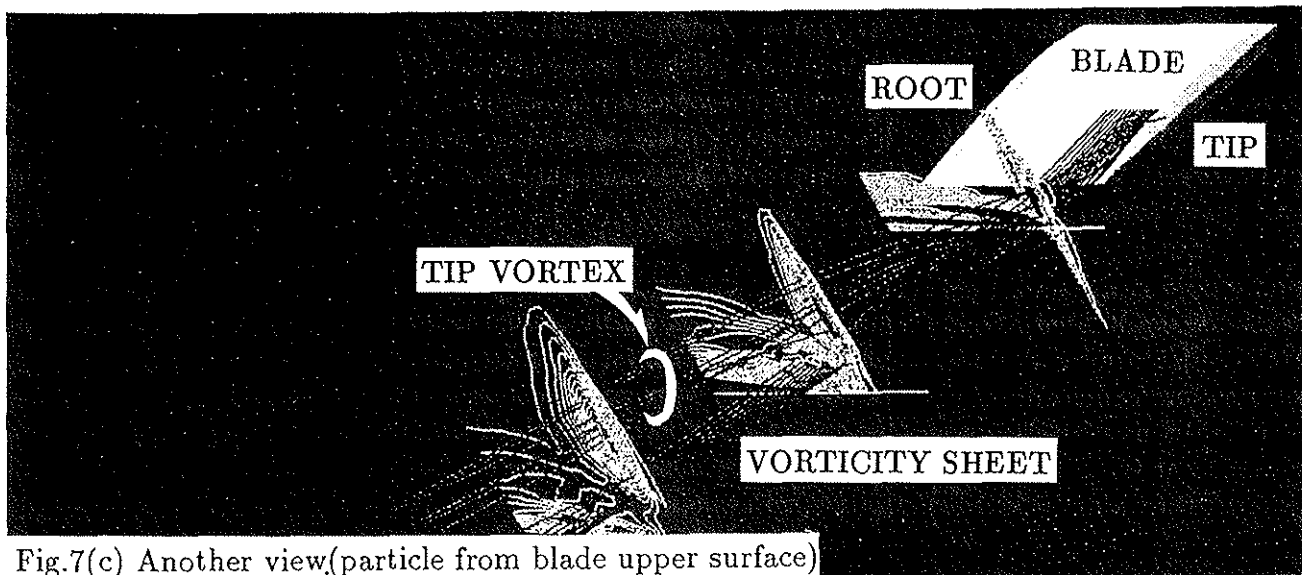
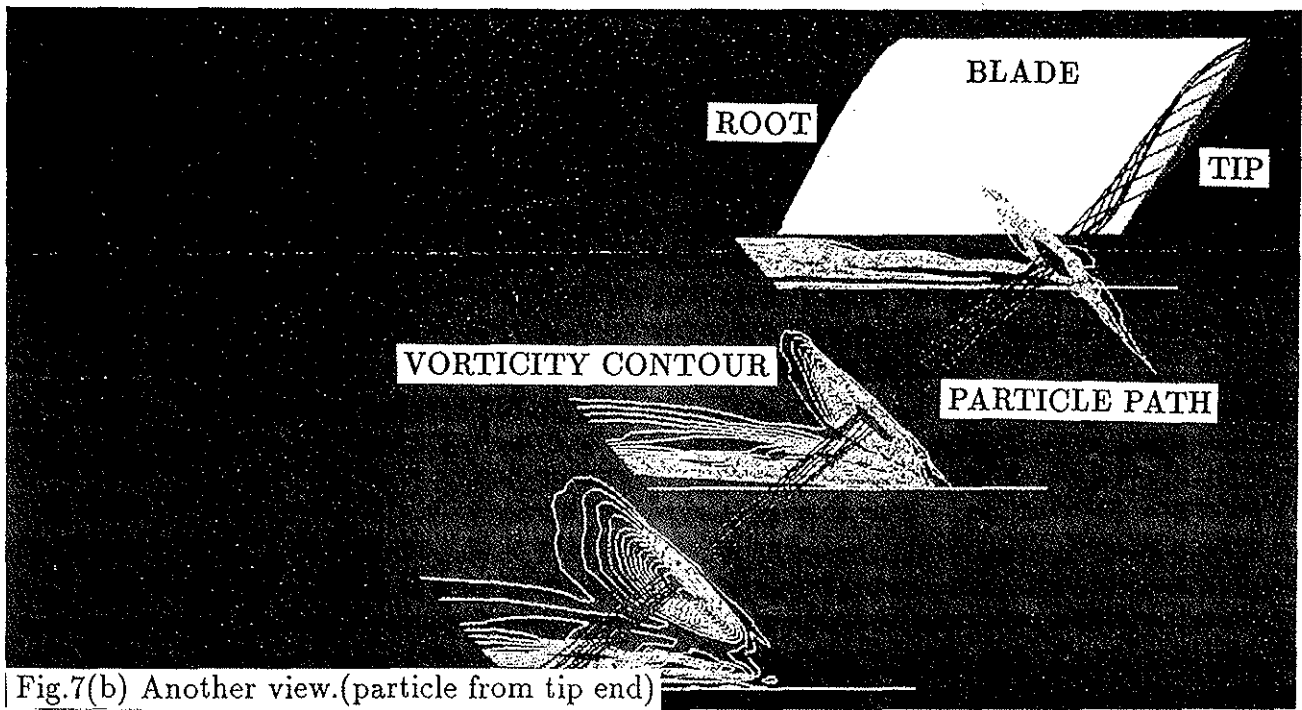
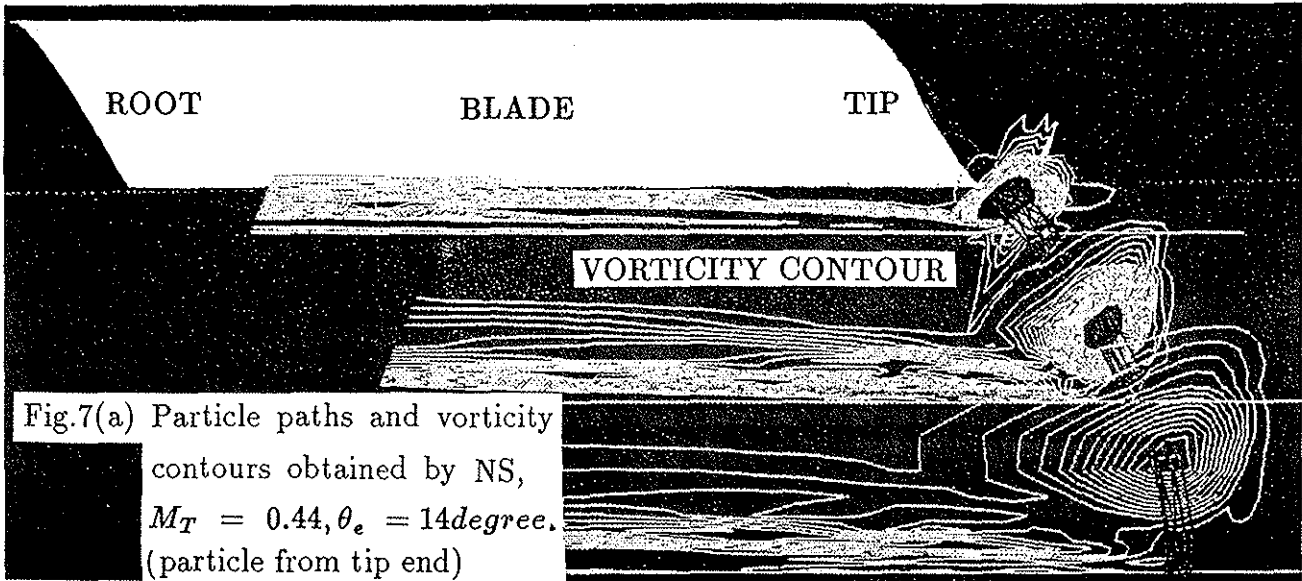


Fig.6 Planes in which vorticity contour is obtained.

focused to analyze the effect of modified tip shapes on the flowfield at the retreating side by solving the Navier-Stokes equations. Therefore, as a basic case, the hovering condition with subsonic ($M_T = 0.44$) and moderate collective pitch angle ($\theta_c = 8.0 \text{ degree}$) is calculated by the present NS code and the results are compared with those of Euler code in order to understand the difference between the results of viscous and inviscid analysis.

Fig.9(a)-(b) show the effect of the blade tip shapes on the aerodynamic performance in



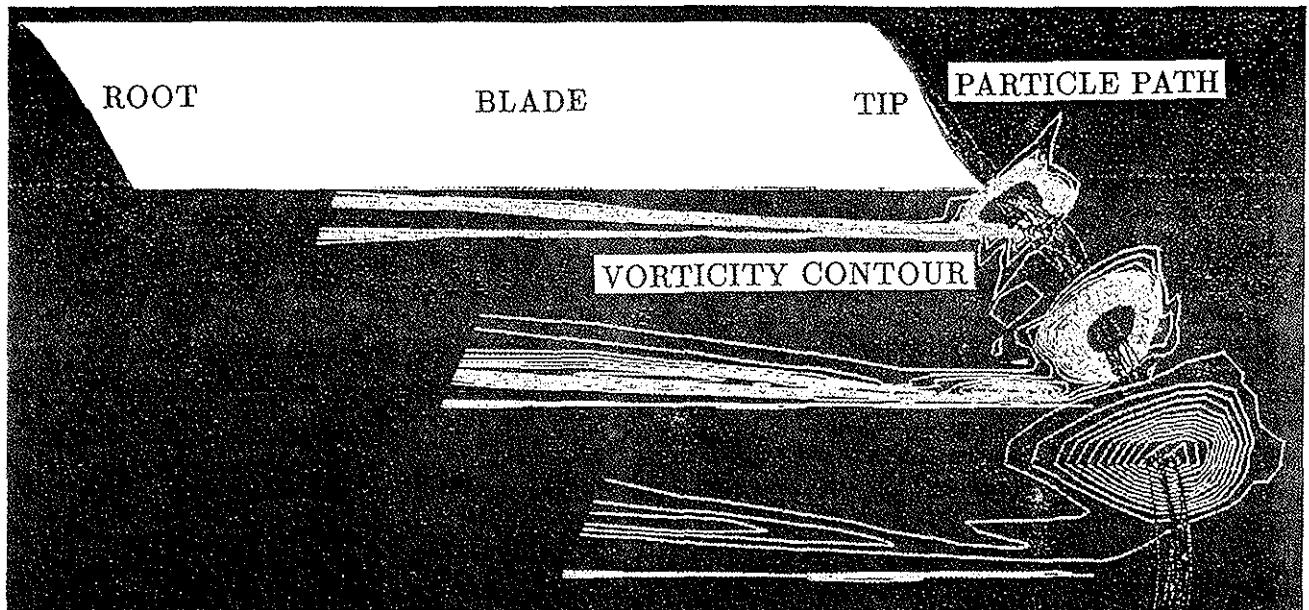


Fig.8 Particle paths and vorticity contours obtained by Euler , $M_T = 0.44, \theta_e = 14 \text{ degree}$.

comparison with NS and Euler calculations. In this figure, C_T and C_Q are the thrust and torque coefficient respectively and σ is the solidity. The subscript 0 means the value of rectangular tip shape. In order to obtain C_T and C_Q , the computational region is extended to the root of a blade in the following calculations. The modified tip shapes have the straight 1/4 chord line and the every blade section is 0012 airfoil section. The dimensions of these tips are given in Table 1.

(1) Swept tip

The different characteristics are observed between NS and Euler analyses. In the NS analysis, the value of C_T/σ is maximum for the straight tip and decreases both for the swept-back and swept-forward tips. The value of C_Q/σ is minimum for the straight tip and increases both for the swept-back and swept-forward tips. In contrast, the both values of C_T/σ and C_Q/σ obtained by the Euler analysis increase as the swept back angle becomes larger. These differences are caused by the development of the three-dimensional boundary-layer, which changes the pressure distributions on the blade surface as well as the profile drag.

(2) Tapered tip

Although the small difference is observed, the similar qualitative characteristics of C_T/σ and C_Q/σ are obtained for the variation of the taper ratio between NS and Euler analyses. Except for the C_T/σ by the NS analysis for

the taper ratio above 1.0 , the value of C_T/σ and C_Q/σ increase as the taper ratio becomes larger.

Euler analysis Fig.10(a)-(b) show the thrust and the torque caused by the modified tip shapes in various tip speeds.

(1) Swept tip

It is observed that C_Q/σ in subsonic condition slightly increase as the sweep-back angle becomes larger(see Fig.10(b)). This is because the larger C_T/σ increases the induced drag(see Fig.10(a)). In contrast, C_Q/σ in transonic condition becomes smaller as the sweep-back angle increases(see Fig.10(a)). This is because the wave drag decreases owing to the reduced intensity of shock wave.

(2) Tapered tip

It is observed that C_Q/σ in subsonic condition becomes larger as the taper ratio increases(see Fig.10(b)). This is because the larger C_T/σ increases the induced drag(see Fig.10(b)). In transonic condition, C_Q/σ shows the different tendency from the subsonic region(see Fig.10(b)) because of the complex mechanism of shock generation near tapered tip. The tapered tip of the taper ratio above 1.0 weakens the intensity of shock wave at the tip end and strengthens it near the station starting the taper. In contrast, the tapered tip of the taper ratio less than 1.0 shows the opposite tendency.

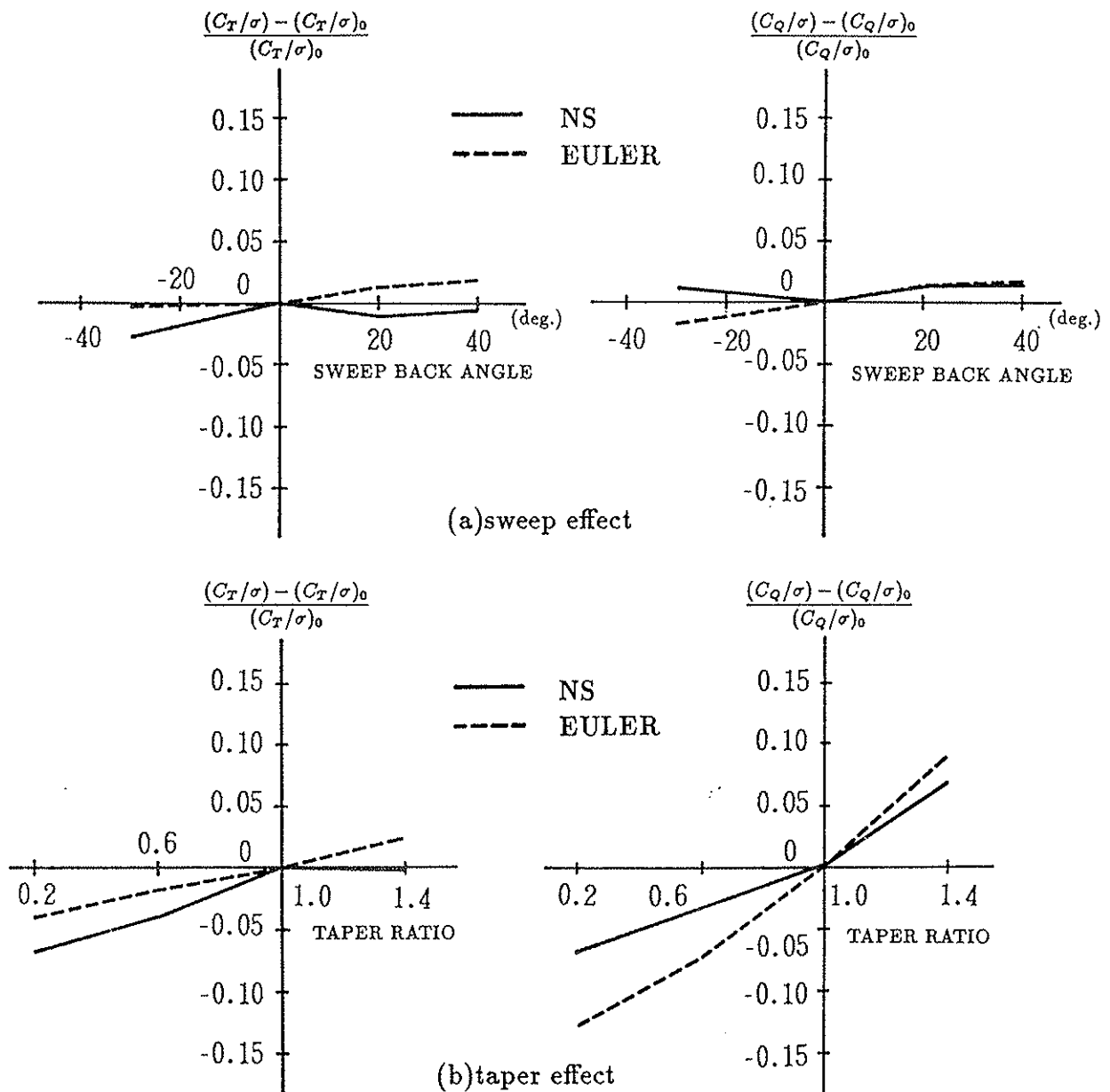


Fig.9 Effect of the blade tip shape on the aerodynamic performance in comparison with NS and Euler calculations.

Table 1 Dimensions of modified tips.

Conclusions

A three-dimensional Navier-Stokes code in conjunction with the $q - \omega$ two-equation turbulence model developed by Coakley is applied to analyze the flowfield around a model helicopter rotor in hover using wake-correction by LCM. As a result, following conclusions are drawn.

- A. The calculated results for rectangular tip shape using the Navier-Stokes code presented here are in good agreement with the measured pressure distributions on

Shape No.	Sweep-back Angle
(S-1)	-30 degree (from $x/R = 0.95$)
(S-2)	20 degree (from $x/R = 0.95$)
(S-3)	40 degree (from $x/R = 0.95$)

Shape No.	Taper Ratio
(T-1)	1.4 (from $x/R = 0.95$)
(T-2)	0.6 (from $x/R = 0.95$)
(T-3)	0.2 (from $x/R = 0.95$)

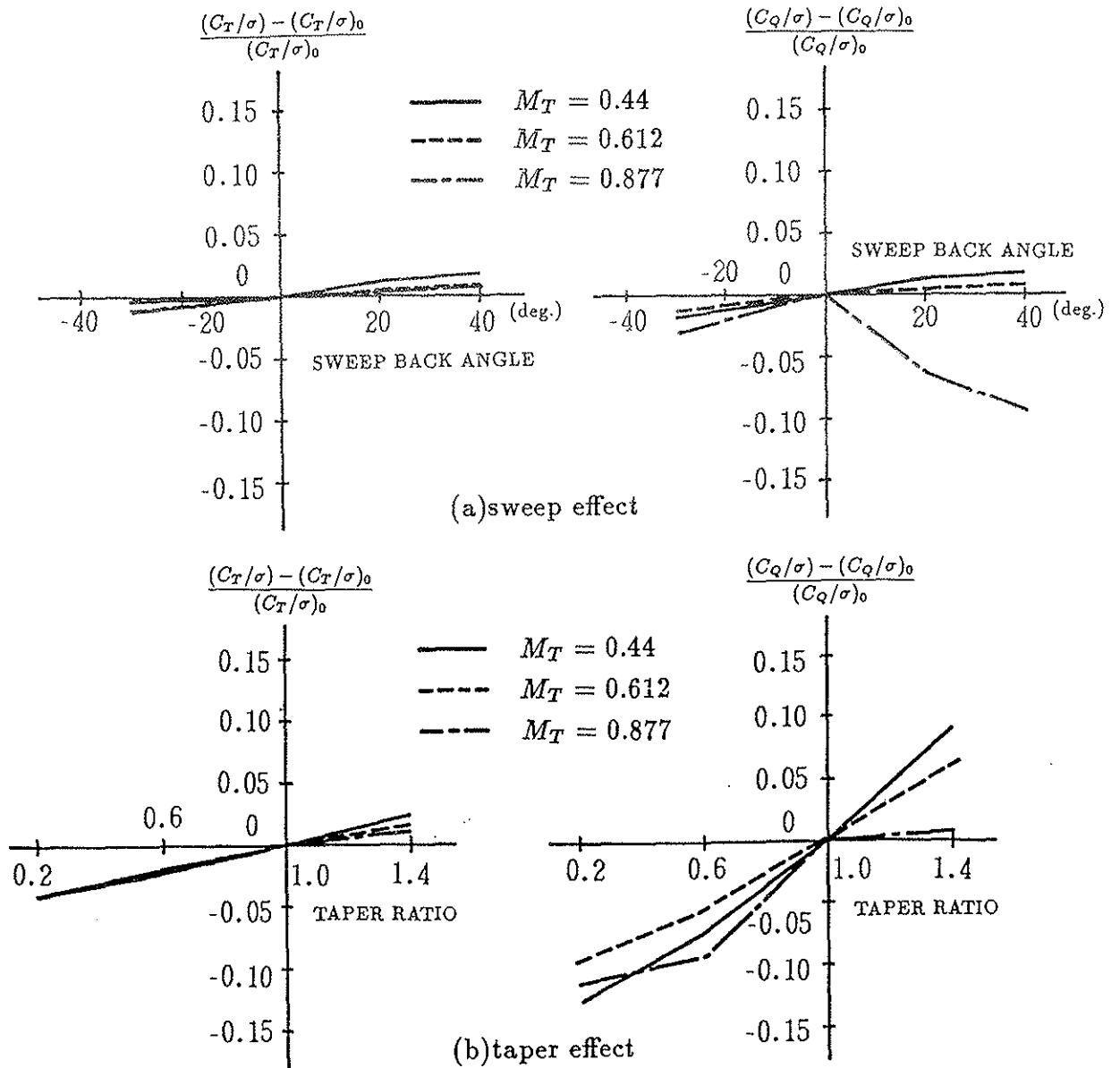


Fig.10 Effect of the blade tip shape on the aerodynamic performance in various tip speed by Euler calculation.

blade surface for both nonlifting and lifting cases.

- B. The estimation of wake effects is important for the analysis of rotor flowfield, and LCM is an effective method for this estimation.
- C. The following results are drawn by NS analysis for swept or tapered tip shapes. For the variation of the sweep back angle, the different characteristics of C_T/σ and C_Q/σ are observed between NS and Euler analyses. This is caused by the development of the three-dimensional boundary-layer on the rotating blade. For the vari-

ation of taper ratio, the similar characteristics of C_T/σ and C_Q/σ are observed between two analyses.

- D. The following results are drawn by Euler analysis for swept or tapered tip shapes. In subsonic condition, C_Q/σ grows as the increase of sweep-back angle or taper ratio, because the larger C_T/σ increases the induced drag. In transonic condition, as the increase of sweep-back angle C_Q/σ becomes smaller because of the reduced intensity of shock wave. In addition, the tendency as the increase of taper ratio in transonic condition is different from in subsonic because of the complex flowfield around tapered tip shape.

References

1. Perry, F.J., "Aerodynamics of the Helicopter World Speed Record," 43rd Annual National Forum of the American Helicopter Society, May, 1987.
2. Caradonna, F.X. and Isom, M.P., "Subsonic and Transonic Potential Flow over Helicopter Rotor Blades," AIAA Journal, Vol.10, No.12, pp 1606-1612, December, 1972.
3. Arieli, R. and Tauber, M.E., "Computation of Subsonic and Transonic Flow about Lifting Rotor Blades," AIAA Paper 79-1667.
4. Chang, I.C. and Tung, C., "Numerical Solution of the Full-Potential Equation for Rotors and Oblique Wings Using a New Wake Model," AIAA Paper 85-0268.
5. Egolf, T.A. and Sparks, S.P., "Hovering Rotor Airload Prediction Using a Full-Potential Flow Analysis with Realistic Wake Geometry," Proceedings of the 41th Annual Form of the AHS, May, 1985.
6. Sankar, N.L. and Prichard, D.S., "Solution of the Transonic Flow Past Rotor Blades Using the Conservative Full-Potential Equations," AIAA Paper 85-5012.
7. Strawn, R.C. and Caradonna, F.X., "Conservative Full-Potential Model for Unsteady Transonic Rotor Flows," AIAA Paper 86-0079.
8. Agarwal, R.K. and Deese, J.E., "Euler Calculation for Flowfield of a Helicopter Rotor in Hover," AIAA Paper 86-1782.
9. Agarwal, R.K. and Deese, J.E., "An Euler Solver for Calculating the Flowfield of a Helicopter Rotor in Hover and Forward Flight," AIAA Paper 87-1427.
10. Chang, I.C. and Tung, C., "Euler Solution of the Transonic Flow for a Helicopter Rotor," AIAA Paper 87-0523.
11. Chen, C.L. and McCroskey, W.J., "Numerical Simulation of Helicopter Multi-Bladed Rotor Flow," AIAA Paper 88-0046.
12. Chen, C.L. McCroskey, W.J. and Obayashi, S., "Numerical Solutions of Forward-Flight Rotor Flow Using an Upwind Method," AIAA Paper 89-1846.
13. Kroll, N., "Computation of the Flow Fields of Propellers and Hovering Rotors Using Euler Equations," 12th European Rotorcraft Forum, Paper No.28, September, 1986.
14. Roberts, T.W. and Murman, E.M., "Solution Method for a Hovering Helicopter Using the Euler Equations," AIAA Paper 85-0436.
15. Sankar, N.L. Wake, B.E. and Lekoudis, S.G., "Solution of the Unsteady Euler Equations for Fixed and Rotor Wing Configurations," AIAA Paper 85-0120.
16. Sankar, N.L. and Tung, C., "Euler Calculations for Rotor Configurations in Unsteady Forward Flight," Proceedings of the 42th Annual National Forum of the AHS, 1986.
17. Agarwal, R.K. and Deese, J.E., "Navier-Stokes Calculations of the Flowfield of a Helicopter Rotor in Hover," AIAA Paper 88-0106.
18. Srinivasan, G.R. and McCroskey, W.J., "Navier-Stokes Calculations of Hovering Rotor Flowfields," Journal of Aircraft Vol.25, No.10, 1988.
19. Wake, B.E. and Sankar, L.N., "Solutions of the Navier-Stokes Equations for the Flow About a Rotor Blade," Journal of the American Helicopter Society, April, 1989.
20. Matuo, Y. et al., "Navier-Stokes Computations for Flowfield of Advanced Turbo-prop," AIAA Paper 88-3094.
21. Matuo, Y. et al., "Navier-Stokes Simulations Around a Propfan Using Higher-Order Upwind Schemes," AIAA Paper 89-2699.
22. Coakley, T.J., "Turbulence Modeling Methods for the Compressible Navier-Stokes Equations," AIAA Paper 83-1693.
23. Azuma, A. Nasu, K. and Hayashi, T., "An Extension of the Local Momentum Theory to the Rotors Operating in a Twist Flow Field," Vertica, Vol.7, No.1, 1983.
24. Chakravarthy, S.R. and Osher, S., "A New Class of High Accuracy TVD Schemes for Hyperbolic Conservation Laws," AIAA Paper 85-0363.
25. Harris, C.D., "Two-dimensional Aerodynamic Characteristics of the NACA 0012 Airfoil in the Langley 8-Foot Transonic

Pressure Tunnel," NASA TM 81927, April, 1981.

26. Caradonna, F.X. and Tung, C., "Experimental and Analytical studies of a Model Helicopter Rotor in Hover," 6th European Rotorcraft and Powered Lift Aircraft Forum, September, 1980.